RSC Advances

PAPER

View Article Online
View Journal | View Issue

Cite this: *RSC Adv.*, 2026, **16**, 24611

Preparation and recrystallization of amorphous L-glutamic acid

Yuhang Liu,[abc] Yuchen Zheng,[b] Ziming Li,[b] Zhihai Wu,[b] Xiong Xiao,[b] Yongming Liu,[d] Wangchuan Xiao,[bc] Fenghua Chen *[bc] and Rongrong Xue *[b]

Amino acids, as essential biological molecules and industrial raw materials, exhibit polymorphic behavior that significantly impacts their physicochemical properties and applications. Non-classical crystallization pathways involving amorphous intermediates are commonly observed in the crystallization process of amino acids including L-glutamic acid (Glu). An effective research approach in the field of non-classical crystallization is to synthesize metastable intermediates to study the crystallization mechanisms. Herein, amorphous Glu was successfully synthesized using $CaCl_2$ as a stabilizer through ball milling (1 : 1 Glu–$CaCl_2$ molar ratio), spray drying (1 : 1 and 2 : 1 ratios) and aqueous evaporation (up to 5 : 1 ratio). The metastable amorphous Glu with high Glu content (87 wt% for the 5 : 1 ratio) was prepared *via* evaporation for the first time. The amorphous nature of the samples was confirmed by powder X-ray diffraction and low-frequency Raman spectroscopy. IR, mid-frequency Raman, and ^{13}C solid-state NMR spectroscopy confirmed the main existence form of Glu neutral zwitterions in the amorphous Glu, while IR and mid-frequency Raman spectroscopy revealed that the structure of the amorphous Glu resembles Glu aqueous solution. Solubility and pH measurements indirectly showed that Glu are coordinated with Ca^{2+}. Suspension recrystallization demonstrated that α polymorph is the primary recrystallization product of the amorphous Glu. The discovery of metastable amorphous intermediates would provide new insights into the non-classical crystallization of amino acids.

Received 7th December 2025
Accepted 7th May 2026

DOI: 10.1039/d5ra09451h

rsc.li/rsc-advances

Introduction

Amino acids, as a class of vital biological small molecules and key industrial raw materials, have a wide range of applications in various industries such as food, pharmaceuticals, and chemicals.[1–3] Amino acid molecules exhibit rich polymorphism phenomenon.[4–6] Different polymorphs show significant differences in physicochemical properties (*e.g.* solubility, biological activity, mechanical strength), and will directly affect the production, performance and application of these products.[7,8] Therefore, precisely controlling the polymorphism of amino acids is of great significance for improving product quality and enhancing market competitiveness.

Non-classical crystallization processes have revealed that crystal growth can be driven by individual molecules or ions, or by larger structural units such as amorphous nanoparticles, crystallized nanoparticles, clusters, liquid precursors, *etc.*[9,10] The amorphous phase is one kind of typical intermediate involved in the non-classical crystallization process.[11–13] In the field of non-classical crystallization of amino acids, amorphous intermediates have been proposed or observed in the case of glycine,[14] alanine,[15,16] proline,[17] L-glutamic acid (Glu),[18–20] *etc.*, which is highly related to the polymorphism control of amino acids. Moreover, in the field of co-amorphous systems for solubilization, amino acids are the most widely used co-formers, offering a promising strategy to enhance the solubility, physical stability, and bioavailability of poorly water-soluble drugs.[21,22] However, macroscopic observation of the amorphous amino acid intermediates with high amino acid content remains unavailable, which limits our understanding of the non-classical crystallization process of amino acids. Research on the amorphous calcium carbonate (ACC) also faced the similar preparation challenge in the early stage, and ACC became a hotspot in the non-classical crystallization field after the successful synthesis of metastable ACC, which enabled detailed characterizations.[23,24] We previously developed a formulation utilizing anhydrous $CaCl_2$ to stabilize amorphous glycine, although we cannot obtain amorphous products with high glycine content.[25]

The anhydrous polymorphs of Glu include stable β polymorph and metastable α polymorph.[26–28] α polymorph is the preferred polymorph from Glu aqueous solution. α polymorph is stable at low temperatures (<222 K), and β polymorph is the most stable at room temperatures.[29] α polymorph can

[a]*School of Chemical Engineering, Fuzhou University, Fuzhou 350116, Fujian, China*
[b]*School of Resources and Chemical Engineering, Sanming University, Sanming 365004, Fujian, China. E-mail: fenghuachen@fjsmu.edu.cn; rongrongxue@fjsmu.edu.cn*
[c]*Fujian Engineering Research Center of Advanced Fluorine-Containing Materials, Sanming University, Sanming 365004, Fujian, China*
[d]*School of Education and Music, Sanming University, Sanming 365004, Fujian, China*

irreversibly transform into β polymorph at 140 °C.[30] In this work, the additive-stabilized strategy was used for preparing amorphous Glu. The preparation method is the key factor for obtaining amorphous Glu with high Glu content. Ball milling method produced amorphous phase with Glu–$CaCl_2$ molar ratio of 1 : 1, spray drying method can prepare samples with Glu–$CaCl_2$ molar ratio of 1 : 1 and 2 : 1, and aqueous evaporation method allowed for the fabrication of amorphous phase with Glu–$CaCl_2$ molar ratios up to 5 : 1. The metastable amorphous Glu with high Glu content (87 wt% for the 5 : 1 ratio) was prepared *via* evaporation for the first time. IR and mid-frequency Raman spectroscopy revealed that the structure of the amorphous Glu resembles Glu aqueous solution. IR, mid-frequency Raman, and ^{13}C solid-state NMR spectroscopy confirmed the main existence forms of Glu in the amorphous samples are Glu neutral zwitterions. The complex of Glu and Ca^{2+} is the main interaction, which is the key factor for the formation amorphous Glu. Solubility and pH measurements indirectly showed that Glu are coordinated with Ca^{2+} in solution. However, spectroscopic analysis method used in this work cannot confirm the coordination interaction between Ca^{2+} and Glu both in the solid state and solution. The amorphous Glu samples can primarily recrystallize into the metastable α polymorph. The preparation of metastable amorphous amino acid intermediates will promote the research on the non-classical crystallization of amino acid.

Experimental part

Materials

L-Glutamic acid ($C_5H_9NO_4$, Glu, 99%), anhydrous calcium chloride ($CaCl_2$, 96%) and bromothymol blue ($C_{27}H_{28}Br_2O_5S$, ACS, dye content 95%) were purchased from Aladdin. NaOH (AR) was bought from Shanghai Hushi. Raw Glu included newly purchased material and long-stored materials in laboratory (Fig. S1a). All reagents were used without any treatments.

Methods

Preparation of Glu polymorphs

α polymorph. Raw Glu is in the form of α polymorph. α polymorph can be prepared through anti-solvent precipitation method by mixing rapidly 30 mL of Glu saturated solution and 30 mL of ethanol under stirring at room temperature. α polymorph can also be prepared through cooling recrystallization method. 1.00 g of raw Glu was dissolved into 20 mL of water at 80 °C, and then the solution was stirred and naturally cooled to room temperature. Precipitates were filtered and dried in air.

β polymorph. 3 g of raw Glu, which was stored for years, was added into 30 mL of water and stirred overnight. The suspension was filtered and dried in air, Glu β polymorph can be obtained. The suspending time can be extended or NaCl can be added as catalyst to ensure the completion of crystal form transformation.

Amorphous Glu

Neat ball milling method. 1.00 g of raw Glu and a certain weight of anhydrous $CaCl_2$ (0.76 g for 1 : 1 Glu–$CaCl_2$ molar ratio, termed as BM-1) were neat ball milled for 2 hours. Ball milling process was conducted on the apparatus (Changsha Tianchuang XQM-1, 220 V, 50 Hz, 670 rpm), using 100 mL stainless steel jars with ~88 g ZrO_2 milling balls (1 *Φ*15 mm, 1 *Φ*12 mm, 7 *Φ*7 mm, 13 *Φ*8 mm, and 63 *Φ*5 mm balls).

Spray drying method. 2.00 g of raw Glu and a certain weight of $CaCl_2$ (1.52 g for 1 : 1 Glu–$CaCl_2$ molar ratio and 0.76 g for 2 : 1 Glu–$CaCl_2$ molar ratio, termed as SD-1 and SD-2, respectively) were completely dissolved into 2 L of deionized water at room temperature. The resulting solution was spray dried (Shanghai Pilotech YC-015, inlet temperature 180 °C, outlet temperature ~110 °C, feed rate 10 mL min^{-1}, atomizing air pressure 24 kg cm^{-1}, drying air flow rate 30 m^3 h^{-1}).

Evaporation method. 1.00 g of raw Glu and a certain weight of $CaCl_2$ (0.76, 0.38, 0.25, 0.19, 0.15 g for 1 : 1, 2 : 1, 3 : 1, 4 : 1, 5 : 1 Glu–$CaCl_2$ molar ratio, termed as EV-1, EV-2, EV-3, EV-4, EV-5, respectively) were added into 100 mL of water. Then, the suspensions were placed on a heated plate at 70 °C to ensure the dissolution of Glu, which was confirmed by observing the Tyndall effect with a laser pointer. A certain volume of the above prepared solutions was dropped onto the aluminum (Al) substrates kept at 150 °C. Specifically, 1.0 mL of the solution was dropped for EV-1, EV-2 and EV-3, and 0.5 mL was dropped for EV-4 and EV-5.

Recrystallization of amorphous Glu. For amorphous Glu obtained through ball milling or spray drying (BM-1, SD-1, and SD-2), 0.50 g of sample was added into 5 mL of water, and then the suspension was stirred for 10 minutes. For amorphous Glu obtained by evaporation, 0.2 mL of water was added onto the surface of the glassy product formed on the Al substrate at room temperature, and then was kept standing for 10 min. The product of the recrystallization process mentioned above was collected by filtering and then was dried in air. Product were collected from five experiments to obtain sufficient amount of sample for testing.

Solubility measurement. The used raw Glu, in the form of α polymorph, was freshly purchased, which is stable in water or in $CaCl_2$ solution overnight at 37 °C. 2.00 g of raw Glu and a certain weight of $CaCl_2$ (0, 0.50, 1.00, 1.50, 2.00, 2.50 g) were added into 100 mL of water at 37 °C. The suspensions were stirred for one day and then was kept standing. 20 mL of the supernatant from each sample was collected and then was titrated by a NaOH standard solution (0.10 M) with bromothymol blue as indicator. The titration experiment was carried out in parallel three times.

pH measurement. For 0.44 mg per mL Glu aqueous solution, pH measurement was conducted under stirring at room temperature. Specifically, 2 mL of 0.50 M $CaCl_2$ solution were added and the solution was stirred for 10 min before measuring the pH. A total of 20 mL of $CaCl_2$ solution was added in several portions, with 2 mL added each time. Each measurement was conducted three times in parallel (Mettler Toledo FiveEasy Plus, ±0.01 pH). For 4.40 mg per mL Glu aqueous solution, the pH measurement was carried out in the same way, except that the concentration of $CaCl_2$ solution used was changed to 5.00 M.

Characterization. Samples were conventionally characterized by powder X-ray diffraction (PXRD, Panalytical X'Pert Pro,

Cu Kα, 40 kV, 30 mA, 5–30°, 4° min^{-1}), scanning electron microscope (SEM, Thermo Fisher Scientific Apreo 2C, 2 kV), attenuated total reflectance Fourier transform IR spectroscopy (ATR-IR, Shimadzu IRAffinity-1S, ATR accessory, 400–4000 cm^{-1}), Raman spectroscopy (Raman, Thermo Fisher Scientific DXR3xi, 532 nm, 40 mW, 0.1 s, 1000 scans, 50–3400 cm^{-1}), and solid state CP-MAS ^{13}C nuclear magnetic resonance (^{13}C ss-NMR, JEOL JNM-ECZ600R, tube diameter 3.2 mm, mas frequency 12 kHz, relaxation delay 3 s, contact time 2 ms, scans 1210). To avoid the amorphous signals from glass substrates, the samples for PXRD test in this work were placed on an Al substrate.

PXRD pattern and morphology simulation. The CIF files were freely downloaded from the Cambridge Crystallographic Data Centre (CCDC). The reported CCDC numbers of Glu α polymorph are LGLUAC02, LGLUAC03, and the CCDC numbers of β polymorph are LGLUAC, LGLUAC01, LGLUAC11, LGLUAC12, LGLUAC14, an LGLUAC15 until October 2025. LGLUAC02 (orthogonal, $P2_12_12_1$, 7.068 × 10.277 × 8.755 Å) of α polymorph and LGLUAC (orthogonal, $P2_12_12_1$, 5.17 × 17.34 × 6.95 Å) of β polymorph were used for simulation. The PXRD pattern simulations were conducted using Mercury software. The morphology was predicted by Materials Studio using BFDH method.

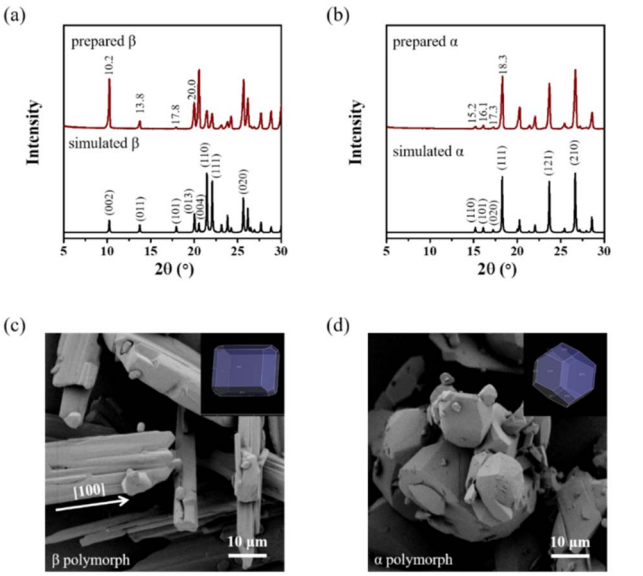

Fig. 1 Preparation of Glu β polymorph *via* suspension crystallization and α polymorph *via* cooling recrystallization. Simulated and experimental powder X-ray diffraction (PXRD) patterns of (a) β polymorph and (b) α polymorph, scanning electron microscope (SEM) images of prepared (c) β polymorph and (d) α polymorph. The inset is the theoretical morphology of Glu β and α polymorph simulated by using Materials Studio.

Result

Polymorph preparation

The anhydrous polymorphs of Glu include stable β polymorph and metastable α polymorph, both of which were reported that can be easily obtained from aqueous solutions.[26–28] The simulated PXRD patterns of β and α polymorphs are different.[31,32] The characteristic peaks are at 10.2°, 13.8°, 17.9°, and 20.0° for β polymorph and at 15.2°, 16.1°, 17.3°, and 18.3° for α polymorph within the 2θ range of 5–20°. β and α polymorph powders with high purity were easily prepared in aqueous environments with good repeatability in our laboratory. Pure β polymorph was obtained by suspending raw Glu (α polymorph) in water (Fig. 1a). The needed suspension time was affected by the purity of raw Glu used (Fig. S1). The existence of trace β polymorph in raw Glu can accelerate the polymorphic transformation. The addition of NaCl can also accelerate the polymorphic transformation process (Fig. S1b). A similar polymorphic transformation process from α-glycine to γ-glycine has been observed with the catalysis effect of NaCl.[33,34] Pure α polymorph can be sourced from the freshly purchased raw Glu or obtained as the cooling recrystallization product of Glu aqueous solution (Fig. 1b). The purity of all the polymorph used in this work was confirmed by the PXRD patterns, compared with the simulated ones.

β polymorph obtained *via* suspension crystallization appeared as rod-like crystals, with the long axis exceeding 100 μm and the size of the other two axes is in the order of 10 μm under SEM observation (Fig. 1c). The rod-like morphology differs from the simulated blocky morphology. The relative intensity of the diffraction peaks in its PXRD pattern suggests the presence of preferred orientation. Compared to the simulated PXRD pattern, the intensity of (002) rises, that of (010) remains, while those of (110) and (111) decline. Thus, we propose that the long axis of the rod-like crystals is approximately aligned with [100].[35] α polymorph obtained through cooling recrystallization presented as nearly spherical crystals,[27] with size in the order of 10 μm, in the SEM image (Fig. 1d). Its morphology is extremely similar to the simulated one, indicating that there is no obvious preferred growth during the crystallization process.

Neat ball milled amorphous Glu

Neat ball milling method was selected here for preparing the amorphous Glu, inspired by the preparation of amorphous $CaCO_3$ with Na_2CO_3 (ref. 36) and amorphous glycine with $CaCl_2$ using neat ball milling.[25] The neat ball milled product of raw Glu is β polymorph with poor crystallinity (Fig. S2, black line), indicating that a solid-state phase transition from α to β has occurred. When the Glu–$CaCl_2$ ratio was 1 : 1 (BM-1), a completely amorphous product can be obtained. Its PXRD pattern shows no peaks at all, not even hump peaks (Fig. 2a). When the Glu–$CaCl_2$ ratio was rose to 2 : 1, the PXRD pattern indicates that the ball milled product is consisted of an amorphous and a crystalline phase. The weak diffraction peaks correspond to α polymorph (*e.g.*, the peak at 18.3°). Thus, neat ball milling process successfully produced an amorphous Glu with the Glu–$CaCl_2$ ratio of 1 : 1 (BM-1). BM-1 appears as a white powder, showing a feature of solid. BM-1 exhibits good thermal stability and storage stability (Fig. 2b). Its PXRD pattern remained unchanged after being heated at 100 °C for 1 h in air

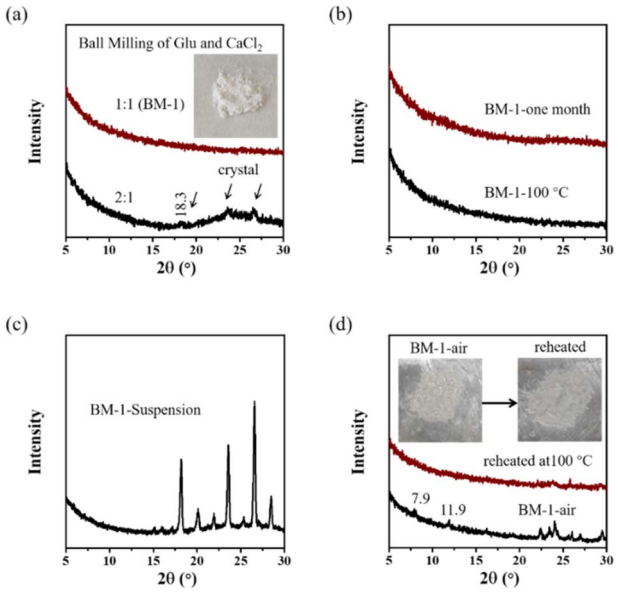

Fig. 2 Preparation, stability and recrystallization of the neat ball milled amorphous Glu with Glu–$CaCl_2$ molar ratio of 1 : 1 (termed as BM-1). (a) PXRD patterns of BM-1 and the neat ball milled product with Glu–$CaCl_2$ molar ratio of 2 : 1, inset is the optical image of BM-1, PXRD patterns of (b) BM-1 after being heated at 100 °C for one hour and BM-1 stored in a sealed tube for one month, (c) aqueous suspension recrystallization product of BM-1, (d) hydrophilic BM-1 kept in air (room temperature, humidity ~60%) overnight and reheated BM-1 (hydrophilic BM-1 was heated at 100 °C for three hours), insets are the optical images of BM-1 in air and reheated BM-1.

or after one month of storage in a sealed tube. BM-1 is unstable in suspension experiment, rapidly transforming into the metastable α polymorph with high purity (Fig. 2c). BM-1 is also unstable in air, which can transform into a solid–liquid mixture (hydrophilic BM-1, Fig. 2d) kept in air overnight, differed from the original solid state, due to the strong hygroscopicity inherited from $CaCl_2$.[37] The related PXRD pattern shows weak crystalline signals at 7.9° and 11.9°, differing from that of β and α polymorphs. When the hydrophilic BM-1 was heated at 100 °C for three hours, the product (reheated BM-1) turned white and its PXRD pattern exhibited the characteristics of amorphous phase. Reheated BM-1 became a hard solid, distinct from its initially powdery appearance. Considering that $CaCl_2$ can form single crystal with neutral biological small molecules, such as cytosine calcium chloride hydrate,[38] diglycine calcium chloride tetrahydrate,[39] we hypothesize that the weak crystalline signals of hydrophilic BM-1 originate from Glu–$CaCl_2$ complex hydrate.

Spray dried amorphous Glu

Spray drying is the most utilized manufacturing processes in the pharmaceutical industry for the preparation of amorphous solid dispersions (ASDs) to enhance the bioavailability of poorly water-soluble drugs.[40,41] The spray drying product of pure Glu aqueous solution is mainly of α polymorph, with a small amount of β polymorph (Fig. S2, red line). Spray drying method was successfully used for the preparation of amorphous Glu with the Glu–$CaCl_2$ of molar ratio 1 : 1 and 2 : 1 (SD-1 and SD-2, Fig. 3a). The PXRD pattern of SD-1 matches BM-1, while that of SD-2 exhibits a hump peak at ~23°. The spray drying product with the Glu–$CaCl_2$ molar ratio of 3 : 1 displays a crystallized PXRD pattern, suggesting a mixture of Glu–$CaCl_2$ complex hydrate, Glu β and α polymorphs. SD-1 and SD-2 demonstrated a good thermal and storage stability, maintaining their PXRD patterns after being heated at 100 °C for 1 hour in air or kept in a sealed tube for one month (Fig. 3b). Both SD-1 and SD-2 were unstable in suspension experiment, and rapidly transformed into a pure metastable α polymorph (Fig. 3c). SD-1 and SD-2 after being kept in air overnight (hydrophilic SD-1 and SD-2) showed the crystalline peaks at 7.9° and 11.9° in their PXRD pattern, which is similar to that of BM-1 kept in air overnight, and the reheated SD-1 and SD-2 showed a significant intensity decrease of the signals at 7.9° and 11.9° (Fig. 3d). The optical images of SD-1 and SD-2 (Fig. S3) were similar to those of BM-1, as well as the property during the hydration process and reheating process. The observed hygroscopicity order is BM-1 > SD-1 > SD-2.

Evaporated amorphous Glu

During the evaporative crystallization process, samples can be obtained by evaporating the liquid with minimal disturbance, which facilitates the formation of amorphous phases.[42] The heating evaporation method was employed to prepare the amorphous Glu with a high Glu–$CaCl_2$ molar ratio at 150 °C.

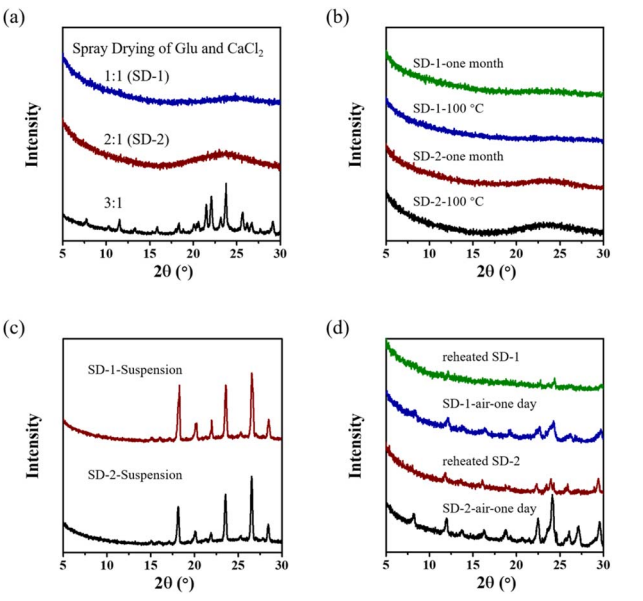

Fig. 3 Preparation, stability and recrystallization of spray dried amorphous Glu with the Glu–$CaCl_2$ ratio of 1 : 1 and 2 : 1, termed as SD-1 and SD-2, respectively. PXRD patterns of (a) SD-1, SD-2, and spray dried product with Glu–$CaCl_2$ molar ratio of 3 : 1, (b) SD-1 and SD-2 after being heated at 100 °C for one hour or stored in a sealed tube for one month, (c) aqueous suspension recrystallization products of SD-1 and SD-2, (d) hydrophilic SD-1 and SD-2 kept in air (room temperature, humidity ~60%) overnight and reheated SD-1 and SD-2 (hydrophilic SD-1 and SD-2 was heated at 100 °C for three hours).

The evaporation product of pure Glu aqueous solution is mainly of the β polymorph, with a small amount of α polymorph (Fig. S2, blue line). The PXRD patterns confirmed that the evaporation products with Glu–$CaCl_2$ molar ratios ranging from 1 : 1 to 5 : 1, termed as EV-1 to EV-5, are completely amorphous (Fig. 4a). The evaporative crystallization with small evaporative volume exhibits good reproducibility for the preparation of amorphous Glu, and increasing the evaporative volume is not beneficial for the formation of amorphous phase. The evaporated amorphous Glu has a high Glu content, *e.g.* 80 mol% (84 wt%) for EV-4 and 83 mol% (87 wt%) for EV-5. It should be noted that the EV samples with even higher Glu content can be synthesized by using a smaller evaporative volume (Fig. S4). *In situ* suspension experiments revealed that EV-1 to EV-5 were all unstable in aqueous environment and transformed into a mixture of α and β polymorphs confirmed by the PXRD patterns (Fig. 4b). α polymorph is stable at low temperatures (<222 K), and β polymorph is the most stable at room temperatures.[29] α polymorph can irreversibly transform into β polymorph at 140 °C.[30] Glu can decompose into poly-Glu above 140 °C with a long-time heating treatment.[30,43] The TG curve of raw Glu (Fig. S5) indicates that it is stable before 180 °C and can decompose at about 190 °C with a heating rate of 10 K min^{-1}. 150 °C was selected here to ensure a fast evaporation rate to ensure the formation of amorphous phase with enough yield. When the samples became dry, the substrates were immediately removed from the heating stage. If the operating temperature drops to 100 °C, the evaporation volume needs to be reduced to 0.05 mL to obtain reproducible amorphous samples (Fig. S6). Considering the operating temperature is 150 °C, it is possible to form β seeds during the preparation process. However, the suspension crystallization products still exhibit a significant amount of α polymorph, showing a recrystallization tendency. EV samples are stable in sealed environment but unstable in air (Fig. S7). All the EV samples would absorb moisture and become sticky after kept in air overnight, which recrystallized showing a mixed signals of mainly complex and β polymorph.

The prepared EV samples exhibit transparent glass appearance (Fig. 5). The surface of the freshly prepared samples is very smooth and hard. It is difficult to crack or scrape them off the substrates using stainless steel tweezers, which makes the characterization of them difficult.

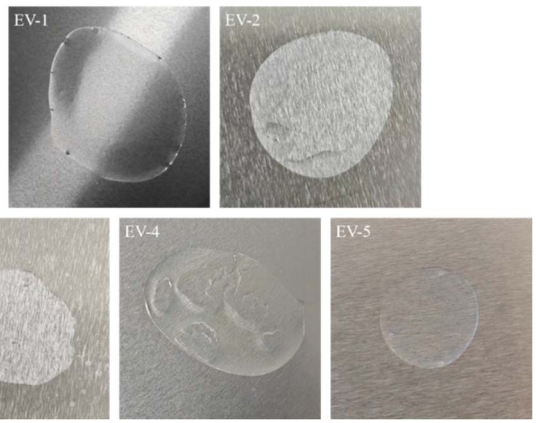

Fig. 5 Optical images of EV-1 to EV-5.

Spectroscopic analysis

The IR spectra of α and β polymorphs are very similar, and most of the IR bands are at the same locations (Fig. 6). The slight differences between α and β polymorphs are that α polymorph has some additional bands, *e.g.* 463, 612, 622 cm^{-1} (arrowed). BM-1 shows very different IR bands compared to those of α and β polymorphs, and lacks comparable signals in the high-frequency region (Fig. S8). The IR spectra of SD-1 and SD-2 are almost same as that of BM-1. The ATR-IR spectra of EV samples were failed to obtain because it is not easy to separate them from the substrates. Typical bands of $CaCl_2$ or $CaCl_2 \cdot 2H_2O$ are not observed in the IR spectra of the amorphous Glu samples (Fig. S9). 15 main bands of BM-1 were selected for comparison (Table 1). Although the spectra of BM-1 and polymorphs are different in visual, many bands in BM-1 are related to those in α and β polymorphs. The main differences between BM-1 and polymorphs are the broad IR bands at 1600 cm^{-1} (double peaks) and 1700 cm^{-1} of BM-1 (arrowed), which are not observed in the polymorphs. Although we did not obtain the IR spectrum of Glu aqueous solution (AQ) because the concentration of Glu is not high enough, the reported Glu aqueous solution also has the two IR bands at 1560 and 1730 cm^{-1}.[44] The assignments of the two bands are COO^- antisymmetric stretching vibration and C=O stretching vibration.[44,45] The IR

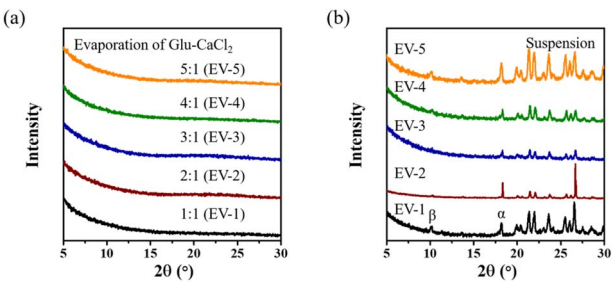

Fig. 4 Preparation and recrystallization of the evaporated amorphous Glu with Glu–$CaCl_2$ molar ratio in the range from 1 : 1 to 5 : 1 termed as EV-1, EV-2, EV-3, EV-4, and EV-5 at 150 °C. PXRD patterns of (a) EV-1 to EV-5, and (b) their suspension recrystallization products.

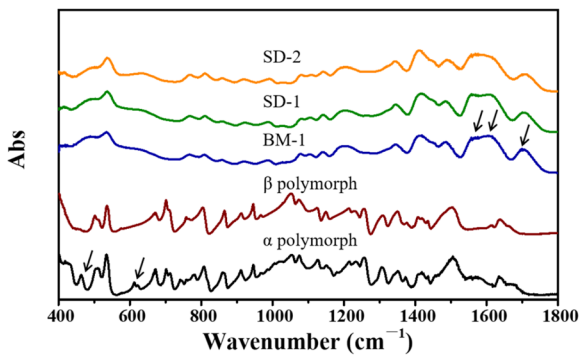

Fig. 6 ATR-IR spectra of α polymorph, β polymorph, BM-1, SD-1, and SD-2 in the range of 400–1800 cm^{-1}.

Table 1 Typical IR bands in the range of 400–1800 cm^{-1} of Glu samples. 15 bands of BM-1 were chosen for comparison

α	β	BM-1	SD-1	SD-2	AQ[44]	Assignment[44,45]
535	536	533	536	536		γ(OCC)
758	760	766	768	768		ρ(CH_2)
807	804	808	810	810		ν(C–C)
860	865	858	858	858		δ(COO^-)
911	910	920	921	920		ν(C–C)
		987	988	991		ν(C–C)
1074	1075	1078	1081	1081		ν(C–O)
1126	1125	1104	1106	1108		δ(NH_3^+)
1150	1150	1141	1142	1143		δ(NH_3^+)
1215	1211	1200	1203	1205	1220	ν(C–O), δ(CH_2)
1351	1350	1345	1345	1344		δ(CH)
1410	1408	1412	1414	1411	1408	ν_s(COO^-)
1506	1504	1485	1486	1486	1451	CH_2 def., δ(CH_2)
		1600	1603	1602	1560	ν_{as}(COO^-), NH_2 def., δ(NH_3^+)
		1700	1700	1699	1730	ν(C=O)

results indicate that the structure of BM-1, as well as SD-1 and SD-2, is similar to that of the Glu aqueous solution and far away from polymorphs.

Low-frequency Raman spectroscopy (*e.g.* <300 cm^{-1}) can distinguish polymorphs, and amorphous phase usually does not have obvious low-frequency Raman bands.[46] α polymorph has typical low-frequency Raman bands at 65, 92, 110, 126, 152 cm^{-1}, β polymorph has typical low-frequency Raman band at 88 cm^{-1}, and Glu aqueous solution show no band (Fig. 7a). BM-1 and the other amorphous Glu (SD-1, 2, EV-1, 2, 3, 4, 5) (Fig. 7a and b) all have no low-frequency band, confirming their amorphous feature.

Mid-frequency Raman spectroscopy can easily distinguish between α and β polymorph (Fig. 8a). For example, α polymorph exhibits bands at 985 and 1077 cm^{-1}, while β polymorph shows a band at 800 cm^{-1}. The mid-frequency Raman spectrum of BM-1 is different from those of polymorphs, and a noticeable increase of the full width at half maximum (FWHM) of the bands is observed. There are only five bands of BM-1 can be observed. The signals assignment of BM-1 reveals that the most bands of BM-1 are highly related to the corresponding bands of α and β polymorphs (Table 2). $CaCl_2$ and $CaCl_2 \cdot 2H_2O$ almost have no signal in the mid-frequency Raman spectra. The most characteristic band of BM-1 is at 1712 cm^{-1}, which is absent in

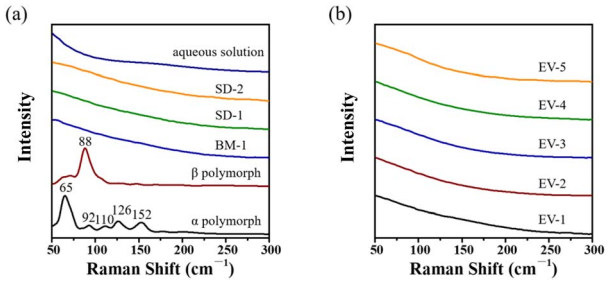

Fig. 7 Low-frequency Raman spectra of (a) α polymorph, β polymorph, BM-1, SD-1, SD-2, and Glu aqueous solution, and (b) EV-1 to EV-5.

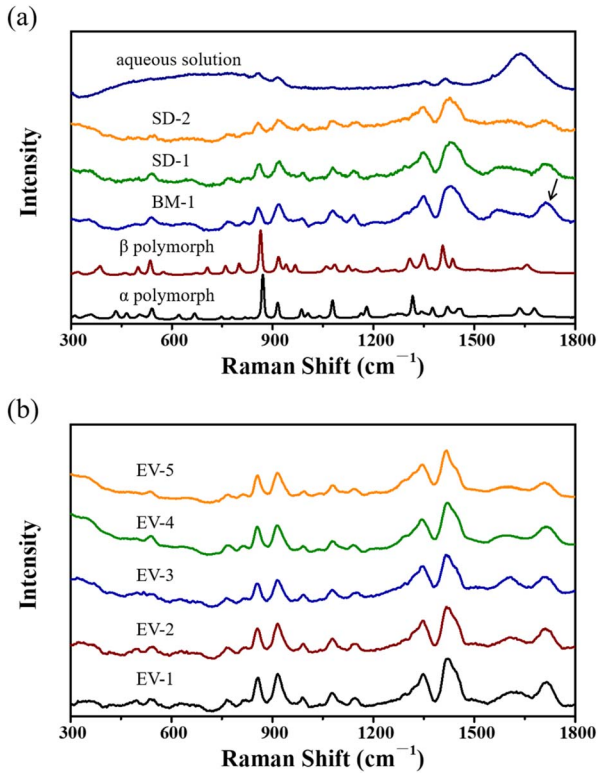

Fig. 8 Mid-frequency Raman spectra of (a) α polymorph, β polymorph, BM-1, SD-1, SD-2, and Glu aqueous solution, and (b) EV-1 to EV-5.

α and β polymorph. The band is assigned to the C=O stretching vibration, mainly belonging to –COOH. The spectrum of Glu aqueous solution has a few observable bands due to the low concentration and Raman activity of Glu. In visual, the spectrum of Glu aqueous solution is close to that of BM-1. By comparison of the band locations, the bands at 812, 856, and 1352 cm^{-1} are close to those of BM-1, suggesting that the structure of BM-1 is similar to Glu solution. The mid-frequency Raman spectra of SD-1, SD-2, and EV-1 to EV-5 are all similar to that of BM-1 (Fig. 8b). The mid-frequency Raman spectra of EV-1 to EV-5 are almost the same, indicating that these signals are basically generated from Glu and the interaction between Glu and Ca^{2+} is not the electrostatic interaction. The high-frequency Raman spectrum of BM-1 also lacks comparable signals (Fig. S10).

Vibrational spectroscopic analysis indicates that the structure of these amorphous Glu samples are close to that of Glu aqueous solution instead of α and β polymorphs. α polymorph is the preferred polymorph in the system of Glu aqueous solution, which can explain the recrystallization tendency of these amorphous Glu samples.

Raw Glu used in this work has a neutral zwitterionic structure, which cannot form salt with Ca^{2+}. The complex of Glu and Ca^{2+} is the main interaction, which is the key factor for the formation amorphous Glu. Spectroscopic analysis method is promising for distinguishing between free Ca^{2+} and the complex. For saturated Glu aqueous solution, its mid-frequency

Table 2 Typical mid-frequency Raman bands in the range of 300–1800 cm^{-1} of Glu samples. 11 bands of BM-1 were chosen for comparison

α	β	BM-1	SD-1	SD-2	EV-1	EV-5	AQ	Assignment[45,47,48]
540	536	540	541	540	536	536		γ(OCC), $\rho(COO^-)$
747	760	765	767	764	765	765		$\rho(CH_2)$
	800	816	814	814	812	813	812	ν(C–C)
870	864	857	861	857	858	857	856	COOH def., $\delta(COO^-)$
914	918	919	919	918	916	914	915	ν(C–C–N), ν(C–C)
985		987	988	989	990	994		ν(C–C)
1077		1079	1079	1081	1077	1079		$\rho(NH_3^+)$, ν(C–O)
		1141	1140	1137	1143	1145		$\tau(CH_2)$, $\delta(NH_3^+)$
1343	1349	1350	1348	1348	1348	1346	1352	$\omega(CH_2)$, δ(CH)
1419	1436	1432	1432	1427	1419	1418	1414	CH_2 def., $\nu_s(COO^-)$
		1712	1711	1711	1713	1713		ν(C=O)

Raman spectrum cannot be distinguished from those of Glu 1% $CaCl_2$ aqueous solution and 10% $CaCl_2$ aqueous solution (Fig. S11), indicating that the existence form of Glu in $CaCl_2$ aqueous solution is mainly Glu neutral zwitterionic. However, the existence of the complex of Glu and Ca^{2+} in solution cannot be confirmed by the vibrational spectroscopic analysis. The salt of Glu and Ca^{2+} was also not observed in the amorphous Glu. The mid-frequency Raman spectra of Glu^- and Glu^+ aqueous solutions have been measured (Fig. S12 and Table S1). It is obvious that Glu neutral zwitterions, Glu^- and Glu^+ have different mid-frequency Raman bands. We did not observe the mid-frequency Raman bands of Glu^- and Glu^+ in the amorphous Glu samples, indicting that Glu zwitterionic is the main existing form of Glu in them. Correspondingly, Ca^{2+} mainly exist as free ions, with a minor of coordinated Glu–Ca complex. The significant differences of the vibrational spectra between amorphous Glu and polymorphs make it hard to determine the interactions between Ca^{2+} and Glu.

^{13}C ss-NMR was used here. The signal to noise ratio (SNR) of α polymorph ^{13}C ss-NMR spectra is not good under our test conditions. The reported ^{13}C ss-NMR spectra of Glu shows both good SNR[49] and poor SNR[50] cases, which may be related to the sample state and the test parameters. The ^{13}C ss-NMR spectrum of β polymorph is highly consistent with the reported one. However, it is difficult to compare α and β polymorphs by the ^{13}C chemical shifts with a small difference (<1.5 ppm). The ^{13}C ss-NMR spectrum of BM-1 exhibits the chemical shifts similar to those of polymorphs with broader peaks due to its amorphous feature (Fig. 9 and Table 3). The chemical shifts of C1 and C5, or C2 and C3 are close, which merge into broad peaks at 178 ppm and 27 ppm, respectively. The shifts of BM-1 at 27 ppm, 55 ppm and 178 ppm were hard to be distinguished from those of α and β polymorphs, proving that Glu in the amorphous Glu samples mainly exist in the form of neutral zwitterions. ^{13}C ss-NMR cannot also determine the interactions between Ca^{2+} and Glu.

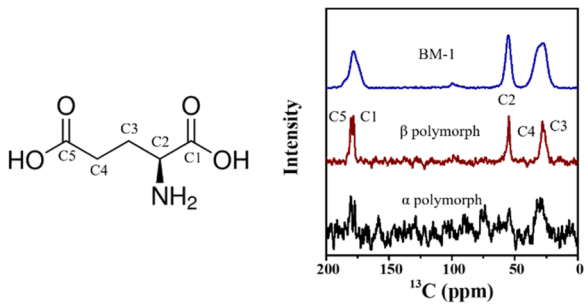

Fig. 9 Solid state CP-MAS ^{13}C nuclear magnetic resonance (ss-NMR) spectra of α polymorph, β polymorph, and BM-1.

Coordination analysis in solutions

Glu ($HOOC–CH_2–CH_2–CH(NH_2)–COOH$) has three p$K_a$ values, 2.2 for $–C_5OOH$, 4.3 for $–C_1OOH$, and 9.7 for $–NH_3^+$.[51] Glu aqueous solution mainly contains three Glu forms as neutral zwitterions, cations (Glu^+), and anions (Glu^-). The δ-pH diagram of Glu (Fig. 10a) reveals that the maximum proportion of Glu neutral zwitterions in water is 85% at the isoelectric point (pI = 3.25) with 7.5% Glu^+ and 7.5% Glu^-. Glu aqueous solution is a complex system, which is unfavourable for the crystallization study on Glu. For the freshly purchased raw Glu (α polymorph), it remains as α polymorph after the solubility test. The solubility of α polymorph is 17.6 mg mL^{-1} at 37 °C (Fig. 10b), similar to the reported ones.[52,53] The addition of $CaCl_2$ can slightly increase the solubility of Glu, reaching 18.6 mg mL^{-1} with 5.0 mg per mL $CaCl_2$ and 20.8 mg mL^{-1} with 25.0 mg per mL $CaCl_2$. Approximately 0.10 mol of Glu will be affected by 1 mol of $CaCl_2$ with $CaCl_2$ concentration in the range of 0 to 25.0. The solubility improvement induced by $CaCl_2$ suggests the formation of complexes, and the limited improvement indicates that the complexes are not very stable. Glu neutral zwitterions contains a carboxylate anion (COO^-) and a carboxyl group (COOH). As an acidic amino acid, the pH of 0.44 mg mL^{-1} and 4.40 mg per mL Glu solutions were measured as 3.61 and 3.35,

Table 3 ^{13}C chemical shifts of Glu in the Glu solids

	$\alpha^{\text{this work}}$	α^{49}	$\beta^{\text{this work}}$	β^{49}	BM-1
C1	177.4	178.4	178.3	178.9	178.4
C5	180.5	179.9	180.3	180.9	
C2	~55	56.1	54.7	55.4	55.0
C3	~30	25.3	26.3	26.7	27.4
C4		29.4	28.0	28.2	

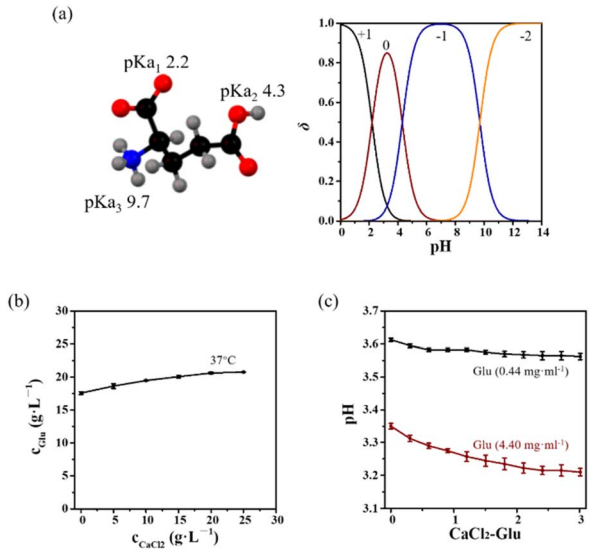

Fig. 10 Coordination analysis between Ca^{2+} and Glu in aqueous solution. (a) pK_a values and the δ-pH diagram of Glu, (b) Glu solubility in water with different $CaCl_2$ concentrations at 37 °C, (c) pH values of 0.44 and 4.40 mg per mL Glu aqueous solution with different $CaCl_2$–Glu molar ratio.

respectively (Fig. 10c). For 0.44 mg per mL Glu aqueous solution, when the molar ratio of $CaCl_2$–Glu is 0.9 : 1 and 1.8 : 1 respectively, the pH value of the solution drops to 3.58 and 3.57. For the system of 4.40 mg mL^{-1}, the pH value decreased to 3.26 and 3.22 with 0.9 : 1 and 1.8 : 1 $CaCl_2$–Glu molar ratios, respectively. In the coordination process, COO^- has a stronger coordination ability than COOH. COO^- of Glu was reported to coordinate with Ca^{2+},[54] and two O atoms of COO^- and one O atom of COOH were also reported to coordinate with Ca^{2+}.[55] The significant decreases of the solution's pH value suggest that COOH may coordinate with Ca^{2+}. The coordination between the COOH and the Ca^{2+} promotes the ionization of H^+ within the carboxyl group.

Discussion

Preparation feasibility of amorphous Glu

The various methods used here to prepare amorphous Glu have distinct advantages and limitations. The amorphous Glu with the Glu–$CaCl_2$ molar ratio of 1 : 1 or 2 : 1 was easy to prepare by ball milling or spray drying method with high yield. The evaporation method can prepare the amorphous Glu with high content of Glu. The production process requires precise controls over factors such as solution volume and evaporation temperature. Briefly, a small solution volume (the key factor) and a relatively high evaporation temperature facilitate the formation of amorphous phase, and the products must be removed promptly to prevent degradation at high temperatures. Another disadvantage of the evaporation method is that the prepared amorphous Glu is difficult to be separated from the substrate. The evaporation method demonstrates the potential of amorphous amino acids as a crystalline intermediate phase, as it was successfully prepared.

Existence form of Glu and the interactions between $CaCl_2$ and Glu

Vibrational spectroscopic analysis indicates that Glu in solutions and the amorphous Glu samples mainly exist in the neutral zwitterionic form. However, spectroscopic analysis method used in this work cannot confirm the coordination interaction between Ca^{2+} and Glu both in the solid state and solution. The solubility and pH test experiment results indicate that Glu are coordinated with Ca^{2+} in solution. Both the COO^- and COOH groups in Glu have the ability to coordinate. But currently, we are unable to determine which groups are coordinated with Ca^{2+}. It is interesting to design suitable amino acid amorphous systems to investigate the interactions between Ca^{2+} and amino acids.

Non-classical crystallization process of Glu

Amorphous Glu has been reported to exist during the Glu non-classical crystallization process,[18–20] but it has not been prepared separately before. Study on the amorphous amino

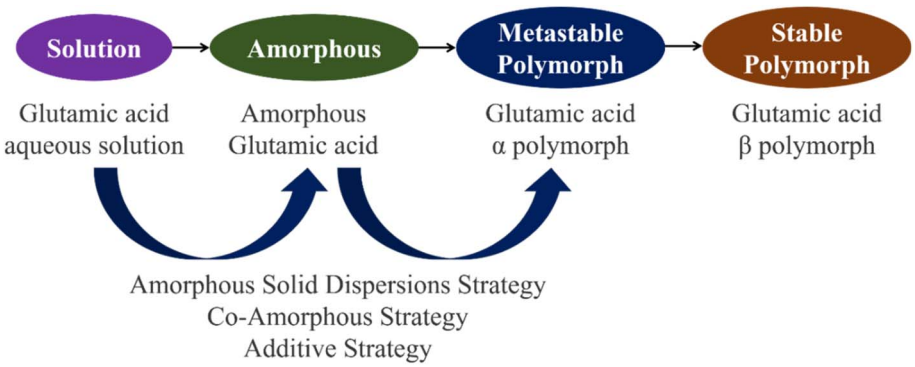

Scheme 1 Schematic of the study on the non-classical crystallization process of Glu *via* amorphous phase intermediate. The amorphous solid dispersions strategy, the co-amorphous strategy or the additive strategy can promote the formation of the amorphous phase and enable the amorphous phase to exist stably.

acids needs to prepare the metastable amorphous amino acids (Scheme 1). The effective strategies can be summarized as amorphous solid dispersions strategy, co-amorphous strategy and additive strategy. The successful preparation of amorphous Glu would enrich the understanding on the non-classical crystallization process of Glu. However, there are still many unknown aspects in our system, *e.g.* the composition and structure of $CaCl_2$–Glu complex hydrate, the polymorph transformation mechanism of amorphous Glu, the coordination between Ca^{2+} and Glu, the structural differences among different amorphous Glu. The current TG results (Fig. S5) reveal that the hygroscopic nature inherited from $CaCl_2$ and the decomposition behaviour of Glu caused significant interference, preventing the samples from drying. The characterization techniques such as DSC, TGA, and water content analysis cannot be performed effectively.

Conclusions

Amorphous Glu was prepared through three methods including ball milling, spray drying, and evaporation. The metastable amorphous Glu with high content of Glu (5 : 1 Glu–$CaCl_2$ molar ratio) was obtained for the first time by evaporation method. IR and Raman spectroscopic analysis indicates that the structure of amorphous Glu is similar to that of Glu aqueous solution. The amorphous Glu tends to transform into α polymorph during the suspension recrystallization process. The preparation of metastable amorphous amino acid intermediates would provide new insights into the non-classical crystallization of amino acids.

Conflicts of interest

There are no conflicts to declare.

Data availability

The data supporting this article have been included as part of the supplementary information (SI). Supplementary information: extended characterization details. See DOI: https://doi.org/10.1039/d5ra09451h.

Acknowledgements

This work was supported by the National Natural Science Foundation of China [Grant No. 22005175], the Industry-University Collaboration Projects in Fujian [Grant No. 2023H6021], and the Natural Science Foundation of Fujian Province [Grant No. 2025J011059 and 2020J01374].

References

1 M. D'Este, M. Alvarado-Morales and I. Angelidaki, *Biotechnol. Adv.*, 2018, **36**, 14–25.
2 A. Bongioanni, M. S. Bueno, B. A. Mezzano, M. R. Longhi and C. Garnero, *Int. J. Pharm.*, 2022, **613**, 121375.
3 M. G. Casteleijn, U. Abendroth, A. Zemella, R. Walter, R. Rashmi, R. Haag and S. Kubick, *Chem. Rev.*, 2025, **125**, 1303–1331.
4 S. A. Moggach, S. Parsons and P. A. Wood, *Crystallogr. Rev.*, 2008, **14**, 143–184.
5 C. H. Görbitz, *Crystallogr. Rev.*, 2015, **21**, 160–212.
6 E. Meirzadeh, I. Weissbuch, D. Ehre, M. Lahav and I. Lubomirsky, *Acc. Chem. Res.*, 2018, **51**, 1238–1248.
7 E. Boldyreva, *Isr. J. Chem.*, 2021, **61**, 828–850.
8 Q. Shi, H. Chen, Y. Wang, J. Xu, Z. Liu and C. Zhang, *Int. J. Pharm.*, 2022, **611**, 121320.
9 J. J. De Yoreo, P. U. P. A. Gilbert, N. A. J. M. Sommerdijk, R. L. Penn, S. Whitelam, D. Joester, H. Zhang, J. D. Rimer, A. Navrotsky, J. F. Banfield, A. F. Wallace, F. M. Michel, F. C. Meldrum, H. Cölfen and P. M. Dove, *Science*, 2015, **349**, aaa6760.
10 J. S. Du, Y. Bae and J. J. De Yoreo, *Nat. Rev. Mater.*, 2024, **9**, 229–248.
11 F. Chen, B. Wu, N. Elad, A. Gal, Y. Liu, Y. Ma and L. Qi, *CrystEngComm*, 2019, **21**, 3586–3591.
12 C. Jia, A. Xiao, J. Zhao, P. Wang, X. Fang, H. Zhang and B. Guan, *Cryst. Growth Des.*, 2024, **24**, 601–612.
13 B. Jin, Z. Liu and R. Tang, *CrystEngComm*, 2020, **22**, 4057–4073.
14 Z. Liao and K. Wynne, *J. Am. Chem. Soc.*, 2022, **144**, 6727–6733.
15 Y. Ma, H. Cölfen and M. Antonietti, *J. Phys. Chem. B*, 2006, **110**, 10822–10828.
16 Y. Ma, H. G. Börner, J. Hartmann and H. Cölfen, *Chem.–Eur. J.*, 2006, **12**, 7882–7888.
17 A. U. Chowdhury, C. M. Dettmar, S. Z. Sullivan, S. Zhang, K. T. Jacobs, D. J. Kissick, T. Maltais, H. G. Hedderich, P. A. Bishop and G. J. Simpson, *J. Am. Chem. Soc.*, 2014, **136**, 2404–2412.
18 C. P. M. Roelands, J. H. ter Horst, H. J. M. Kramer and P. J. Jansens, *AIChE J.*, 2007, **53**, 354–362.
19 T. T. H. Trinh, C. Q. Khuu, S. E. Wolf and A.-T. Nguyen, *J. Cryst. Growth*, 2020, **544**, 125727.
20 T. T. H. Trinh, P. I. Schodder, B. Demmert and A.-T. Nguyen, *Chem. Eng. Res. Des.*, 2021, **169**, 176–188.
21 D. U. Kapoor, S. Singh, P. Sharma and B. G. Prajapati, *AAPS PharmSciTech*, 2023, **24**, 253.
22 A. Saberi, M. Kouhjani, D. Yari, A. Jahani, K. Asare-Addo, H. Kamali and A. Nokhodchi, *J. Drug Delivery Sci. Technol.*, 2023, **86**, 104746.
23 Y.-Q. Niu, J.-H. Liu, C. Aymonier, S. Fermani, D. Kralj, G. Falini and C.-H. Zhou, *Chem. Soc. Rev.*, 2022, **51**, 7883–7943.
24 J. Jiang, P. Yan, C. Liu, T. Sun, S. Xu and Q. Li, *Adv. Powder Technol.*, 2025, **36**, 104850.
25 F. Chen, N. Man, C. Yang, R. Cao, Y. Lian, J.-H. Zhang, W. Lai, R. Xue and Y. Ma, *J. Pharm. Sci.*, 2021, **110**, 3171–3175.
26 S. Liang, X. Duan, X. Zhang, G. Qian and X. Zhou, *RSC Adv.*, 2016, **6**, 74700–74703.
27 H. Shi, F. Li, X. Huang, T. Wang, Y. Bao, Q. Yin, C. Xie and H. Hao, *Ind. Eng. Chem. Res.*, 2020, **59**, 6102–6111.

28 R. Achermann, A. Košir, B. Bodák, L. Bosetti and M. Mazzotti, *Cryst. Growth Des.*, 2023, **23**, 2485–2503.
29 M. T. Ruggiero, J. Sibik, J. A. Zeitler and T. M. Korter, *J. Phys. Chem. A*, 2016, **120**, 7490–7495.
30 H. Wu, N. Reeves-McLaren, S. Jones, R. I. Ristic, J. P. A. Fairclough and A. R. West, *Cryst. Growth Des.*, 2010, **10**, 988–994.
31 S. Hirokawa, *Acta Crystallogr.*, 1955, **8**, 637–641.
32 N. Hirayama, K. Shirahata, Y. Ohashi and Y. Sasada, *Bull. Chem. Soc. Jpn.*, 1980, **53**, 30–35.
33 L. Ding, S. Zong, L. Dang, Z. Wang and H. Wei, *CrystEngComm*, 2018, **20**, 164–172.
34 G. Cotting, O. Urquidi, C. Besnard, J. Brazard and T. B. M. Adachi, *Proc. Natl. Acad. Sci. U. S. A.*, 2025, **122**, e2419638122.
35 N. Garti and H. Zour, *J. Cryst. Growth*, 1997, **172**, 486–498.
36 S. Leukel, M. Panthöfer, M. Mondeshki, G. Kieslich, Y. Wu, N. Krautwurst and W. Tremel, *Chem. Mater.*, 2018, **30**, 6040–6052.
37 Y. Liu, W. Xu, X. Zhou, A. Perwez, G. Qin and X. Zheng, *Small*, 2025, **21**, 2502386.
38 K. Ogawa, M. Kumihashi, K. Tomita and S. Shirotake, *Acta Crystallogr., Sect. B*, 1980, **36**, 1793–1797.
39 K. Jayalakshmi and M. Vijayan, *Acta Crystallogr.*, 1967, **23**, 669.
40 A. Singh and G. Van den Mooter, *Adv. Drug Delivery Rev.*, 2016, **100**, 27–50.
41 D. E. Moseson, T. B. Tran, B. Karunakaran, R. Ambardekar and T. N. Hiew, *Int. J. Pharm.:X*, 2024, **7**, 100259.
42 X. Cheng, X. Chen, C. Liang, H. Jin, S. Ren, R. Xue and F. Chen, *Vib. Spectrosc.*, 2023, **127**, 103565.
43 Z. Zhu, Y. Bian, X. Zhang, R. Zeng and B. Yang, *Spectrochim. Acta, Part A*, 2022, **275**, 121150.
44 F. Zhang, T. Liu and R. Guan, *Spectrosc. Spectral Anal.*, 2017, **37**, 3011–3015.
45 P. Dhamelincourt and F. J. Ramírez, *J. Raman Spectrosc.*, 1991, **22**, 577–582.
46 Y. Fan, R. Xue and F. Chen, *Vib. Spectrosc.*, 2024, **130**, 103626.
47 H. F. Shurvell and F. J. Bergin, *J. Raman Spectrosc.*, 1989, **20**, 163–168.
48 K. Edalati, J. Hidalgo-Jiménez, T. T. Nguyen, M. Watanabe and I. Taniguchi, *Adv. Eng. Mater.*, 2024, **26**, 2302267.
49 Y. Wang, D. Wilson and G. S. Harbison, *Cryst. Growth Des.*, 2016, **16**, 625–631.
50 H. Bachoua, G. Renaudin, B. Badraoui, F. Leroux, M. Debbabi and J.-M. Nedelec, *J. Sol-Gel Sci. Technol.*, 2016, **78**, 621–631.
51 F. Šebesta, Ž. Sovová and J. V. Burda, *J. Phys. Chem. B*, 2024, **128**, 1627–1637.
52 N. C. S. Kee, R. B. H. Tan and R. D. Braatz, *Cryst. Growth Des.*, 2009, **9**, 3044–3051.
53 M. Khellaf, C. Charcosset, D. Mangin and E. Chabanon, *J. Cryst. Growth*, 2021, **570**, 126238.
54 F. Xiang, P. Li, S. Yan, L. Sun, R. I. Cukier and Y. Bu, *New J. Chem.*, 2006, **30**, 890–900.
55 F. Xiang, Y. Bu, H. Ai and P. Li, *J. Phys. Chem. B*, 2004, **108**, 17628–17638.